SI Appendix

Mechanistic insights into electrochemical reduction of CO_2 over Ag using density functional theory and transport models

Meenesh R. Singh[a,b,1], Jason D. Goodpaster[a,c,1], Adam Z. Weber[a], Martin Head-Gordon[a,d], and Alexis T. Bell[a,e,2]

S1. Continuum Transport Model

Figure 1a shows a schematic of a one-dimensional electrochemical cell for reduction of CO_2 and H_2O. The cell has a well-mixed anolyte and catholyte regions to which CO_2 is constantly supplied at 1 atm pressure and 20 sccm flow rate. The Pt anode is used for oxidation of H_2O to O_2 and the Ag(110) cathode is used for reduction of CO_2 to CO. The distance between anode/cathode and the membrane is ~3.56 cm. The anolyte and catholyte are separated by an anion-exchange membrane such as Selemion AMV of 100 μm thickness. The species in the CO_2 equilibrated electrolyte are dissolved CO_2, bicarbonate anions (HCO_3^-), carbonate anions (CO_3^{2-}), protons (H^+), hydroxide anions (OH^-), and metal cation (K^+). The pH of the electrolyte is 6.8 and the concentration of metal cation is 0.1 M.

S1.1 Polarization Losses

Polarization loss due to the transport of species (by migration and diffusion) and concentration gradients can be represented as a sum of i) ohmic loss, ii) diffusion loss, and iii) Nernstian loss. The ohmic loss is due to the resistance of the electrolyte, and the diffusion loss originates from the ionic gradient in the boundary layer near each electrode due to the applied current density. The ohmic and diffusion losses can be combined into the solution loss such that

$$\Delta\phi_{\text{solution}} = \underbrace{\int \frac{i_l}{\kappa} dx}_{\Delta\phi_{\text{ohmic}}} + \underbrace{\sum_i \int \frac{F z_i D_i \nabla c_i}{\kappa} dx}_{\Delta\phi_{\text{diffusion}}} \quad (1)$$

where i_l is the electrolyte current density, κ is the electrolyte conductivity, x is the position, F is Faraday's constant, z_i is the charge number, D_i is the diffusion coefficient, and c_i is the concentration of the i^{th} species. The ionic gradients alter the concentrations of reacting species next to the electrode surfaces (e.g., protons, hydroxide anion, and dissolved CO_2) away from those present in the bulk. This causes an increase in the equilibrium potential of the oxygen evolution

reaction (OER) and the CO_2 reduction reaction (CO2RR), which are referred to collectively as the Nernstian loss. The Nernstian loss is a sum of losses due to differences in pH at the two electrodes, and differences in concentration of CO_2 at the cathode and in the bulk electrolyte is given by

$$\Delta\phi_{\text{Nernstian}} = \underbrace{\frac{2.303RT}{F}\left(\text{pH}_{\text{cathode}} - \text{pH}_{\text{bulk}}\right)}_{\Delta\phi_{\text{cathode pH}}} + \underbrace{\frac{2.303RT}{F}\left(\text{pH}_{\text{bulk}} - \text{pH}_{\text{anode}}\right)}_{\Delta\phi_{\text{anode pH}}} + \underbrace{\frac{RT}{nF}\ln\left(\frac{p_{\text{CO}_2,\text{ bulk}}}{p_{\text{CO}_2,\text{ cathode}}}\right)}_{\Delta\phi_{\text{cathode CO}_2}} \quad (2)$$

where R is the gas constant, T is the temperature, n is the moles of electron transferred per mole of CO_2, and p_{CO_2} is the partial pressure of CO_2. The losses given by Equation (1) and (2) are due to the transport of species in the electrolyte, which, in turn, depend on the applied current density, electrolyte composition, electrolyte hydrodynamics, CO_2 feed concentration and rate, membrane composition, and catalyst selectivity. The kinetic overpotentials for the OER and CO2RR also contribute to the total losses in the electrochemical cell.

S1.2 Acid-Base Equilibria

The amount of CO_2 dissolved in the electrolyte depends on the pressure and temperature of the electrolyte. The equilibrium of CO_2 between gas and liquid phase,

$$\text{CO}_{2(\text{g})} \rightleftharpoons \text{CO}_{2(\text{aq})} \quad (3)$$

is given by Henry's constant (K_0), such that

$$K_0 = \frac{c_{\text{CO}_2}}{f_{\text{CO}_2}} \quad (4)$$

where c_{CO_2} is the concentration of dissolved CO_2, and f_{CO_2} is the fugacity of CO_2 in the gas phase. The dependence of the Henry's constant on the temperature (T, in Kelvin) at ambient pressure is given as(1)

$$\ln\left(K_0\right) = 93.4517\left(\frac{100}{T}\right) - 60.2409 + 23.3585\ln\left(\frac{T}{100}\right) \quad (5)$$

The dissolved CO_2 can also be hydrated to form carbonic acid, but its concentration is only about 1/1000 of the concentration of dissolved CO_2.(2) Therefore, we do not distinguish between the hydrated and dissolved CO_2, and consider them as a single species. The dissolved CO_2 dissociates to produce bicarbonate and carbonate ions when pH is greater than 5. The corresponding pair of reactions is given as

$$\text{CO}_{2(\text{aq})} + \text{H}_2\text{O} \underset{k_{-1}}{\overset{k_{+1}}{\rightleftharpoons}} \text{H}^+ + \text{HCO}_3^-, \quad \text{pK}_1 = 6.37 \quad (6)$$

$$HCO_3^- \underset{k_{-2}}{\overset{k_{+2}}{\rightleftharpoons}} H^+ + CO_3^{2-}, \quad pK_2 = 10.25 \tag{7}$$

The values of the forward rate constants of reactions (6) and (7) are $k_{+1} = 3.71\times10^{-2}\ s^{-1}$ and $k_{+2} = 59.44\ s^{-1}$, respectively.(3) The reverse rate constants can be obtained from pK_1 and pK_2 for reactions (6) and (7), respectively. We also include the bulk ionization of H_2O,

$$H_2O \underset{k_{-w}}{\overset{k_{+w}}{\rightleftharpoons}} H^+ + OH^- \tag{8}$$

The value of the forward rate constant of H_2O ionization is $k_{+w} = 2.4\times10^{-5}\ mol\,L^{-1}\,s^{-1}$ and the equilibrium constant is $K_w = 1\times10^{-14}\ mol^2\,L^{-2}$.(4)

S1.3 Transport of Species in the Electrolyte and Membrane

The transport of species in the electrolyte and membrane must satisfy mass conservation, such that

$$\frac{\partial c_i}{\partial t} + \frac{\partial N_i}{\partial x} = R_i \tag{9}$$

where N_i is the molar flux, and R_i is the volumetric rate of formation of species i (CO_2, HCO_3^-, CO_3^{2-}, H^+, and OH^-). The rate of production of species i, R_i, can be determined from reactions (6) , (7), and (8). The molar flux of species in the dilute electrolyte can be written as a sum of fluxes due to diffusion and migration.

$$N_i = -D_i \frac{\partial c_i}{\partial x} - z_i u_i F c_i \frac{\partial \phi_l}{\partial x} \tag{10}$$

where u_i is the mobility of ion given by the Nernst-Einstein relationship, and ϕ_l is the electrolyte potential. The diffusion coefficients of species in the dilute electrolyte are given in Table S1. We neglect the variation of diffusion coefficients with the electrolyte concentration, as the variation is marginal for dilute electrolytes (<< 10 mol%).(5)

The electrolyte current density i_l can be obtained from the total ionic flux,

$$i_l = F \sum_i z_i N_i \tag{11}$$

and the assumption of electro-neutrality,

$$\sum_i z_i c_i = 0 \tag{12}$$

The same set of Equations [(9) - (12)] were used to model the boundary layer region, the well-mixed region, and the membrane. Expressions for the rate of CO_2 transfer to or from the electrolyte, and diffusion coefficients for transport of ions through the membrane are discussed in the next three subsections.

Table S1: Diffusion coefficients of species in H_2O at infinite dilution at 25℃ (6, 7)

Species	**Diffusion Coefficient (10^{-9} m^2 s^{-1})**	**Mobility (10^{-7} m^2 V^{-1} s^{-1})**
CO_2	1.91	-
HCO_3^-	1.185	0.462
CO_3^{2-}	0.923	0.359
H^+	9.311	3.626
OH^-	5.273	2.054
K^+	1.957	0.762

Well-Mixed Electrolyte

The well-mixed region of the electrolyte, as shown in Figure 1a, was assumed to have no diffusional resistance and therefore charged species are transported only by migration. The net rate formation of HCO_3^-, CO_3^{2-}, H^+, OH^- were set to zero in the bulk because reactions 6, 7, and 8 were assumed to be at equilibrium. Therefore, only the rate of CO_2 transfer from gas phase to liquid phase was non-zero. A constant feed of CO_2 in the well-mixed region was included as an additional generation term on the right side of Equation (9), given as

$$R_{\mathrm{CO_2,\,feed}} = k_l a \left(K_0 f_{\mathrm{CO_2}} - c_{\mathrm{CO_2}} \right) \tag{13}$$

where $k_l a$ (s^{-1}) is the volumetric mass-transfer coefficient on the liquid side of the gas-liquid interface, and $c_{\mathrm{CO_2}}$ (mol/m^3) is a concentration of dissolved CO_2 in the bulk electrolyte. The value of mass transfer coefficient for CO_2 gas-liquid mass transfer in bicarbonate electrolyte is 1.75×10^{-5} m s^{-1}.(8) The measured value of the average radius of CO_2 bubbles emerging from frit is 0.2 mm. Therefore, the value of the volumetric mass-transfer coefficient $k_l a$ is 0.26 s^{-1}. The boundary layer thickness of ~40 μm was chosen according to the limiting current density of CO2RR over Ag.(9)

Membrane

The anion exchange membrane (AEM) such as Selemion AMV was modeled as a solid electrolyte of 100 μm thickness with a fixed concentration of background positive charge of 1

M.(10) The diffusion coefficients of anions and cations were reduced by a factor of 10 (ref. (11)) and by a factor of 100 (assumed), respectively, relative to those in the liquid electrolyte.

S1.4 Charge-Transfer Reactions at Anode and Cathode

The charge-transfer kinetics at the Pt anode was modeled using the Tafel kinetics, such as

$$i_s = i_l = i_R = i_0 \exp\left(\frac{\alpha F \eta}{RT}\right) \tag{14}$$

where i_s is the electrode current density, i_R is the reaction current density, i_0 is the exchange-current density, and α is the transfer coefficient. The kinetic overpotential of a catalyst is given by $\eta = \phi_s - \phi_l - E^0 + \Delta\phi_{\text{Nernstian}}$, where E^0 is the equilibrium potential of the half-reaction at a standard condition and, ϕ_s is the electrode potential.

The half-cell reaction at the Pt anode is the oxidation of H_2O, which produces O_2.

$$\mathrm{H_2O} \rightarrow \frac{1}{2}\mathrm{O_2} + 2\mathrm{H^+} + 2\mathrm{e^-}, \quad E^0 = 1.229\,\mathrm{V} \tag{15}$$

The kinetic parameters for OER over Pt were obtained from Birss and Damjanovic.(12) The exchange current density and transfer coefficient for OER are 4.684×10^{-9} mA cm^{-2} and 0.5, respectively.

The other half-cell reactions over Ag cathode involves the reduction of CO_2 and H_2O to H_2 and CO.

$$\begin{aligned} 2\mathrm{H_2O} + 2\mathrm{e^-} &\rightarrow \mathrm{H_2} + 2\mathrm{OH^-} \qquad E^0 = 0\,\mathrm{V} \\ \mathrm{CO_2} + \ \mathrm{H_2O} + 2\mathrm{e^-} &\rightarrow \mathrm{CO} + 2\mathrm{OH^-} \qquad E^0 = -0.10\,\mathrm{V} \end{aligned} \tag{16}$$

The kinetics of CO2RR and HER over Ag(110) was described using the microkinetic model discussed in Section S2.

S1.5 Electrode Current Density

The current density at a metal electrode is given by Ohm's law:

$$i_s = -\kappa_s \frac{\partial \phi_s}{\partial x} \tag{17}$$

where κ_s is the conductivity of the electrode. To maintain electroneutrality, the divergence of current density in the solid and the liquid was set to zero:

$$\frac{\partial i_l}{\partial x} = 0, \quad \frac{\partial i_s}{\partial x} = 0 \tag{18}$$

The potential in the electrochemical cell was calculated relative to the zero potential of the electrolyte at the cathode-electrolyte interface.

Equations (1) - (18) were solved using COMSOL Multiphysics 4.3b to calculate pH and CO_2 concentration at the cathode as a function of partial current densities of H_2 and CO obtained from the microkinetic model.

S2. Microkinetic Model

Figure 2 shows the mechanism of HER over Ag(110) given by Volmer and Heyrovsky steps.

(Volmer Step) $$** H_2O + e^- \underset{k_{-3}}{\overset{k_3}{\rightleftharpoons}} *H + * + OH^- \tag{19}$$

(Heyrovsky Step) $$H_2O + *H + e^- \underset{k_{-4}}{\overset{k_4}{\rightleftharpoons}} *H_2 + OH^- \tag{20}$$

The rate expressions for Volmer and Heyrovsky steps are given as

$$r_3 = k_3\left[\theta_{**H_2O} - \frac{1}{K_3}\theta_{*H}\,\theta_{*}\,x_{OH^-}\right] \tag{21}$$

$$r_4 = k_4\left[\theta_{*H} - \frac{1}{K_4}\theta_{*H_2}\,x_{OH^-}\right] \tag{22}$$

where θ_s is the fractional coverage of species *s* on the cathode, x_{OH^-} is the mole fraction of OH^- in the electrolyte at the cathode interface, k_i is the forward rate constants, and K_i is the equilibrium constant of the *i*th elementary reaction. The forward rate constants were obtained using the Transition State Theory,

$$k_i(V) = \frac{k_B T}{h} c_* \exp\left[-\frac{\Delta G_i^{\ddagger}(V)}{k_B T}\right] \tag{23}$$

where V is the applied potential, k_B is the Boltzmann constant, T is the temperature of the cell, h is the Planck constant, c_* is the total surface concentration of free sites on Ag(110), and $\Delta G_i^{\ddagger}$ is the free energy of activation of the *i*th reaction. The total concentration of active sites on Ag(110) was $c_* = 7.04\times10^{-6}$ mol m^{-2}. The values of $\Delta G_i^{\ddagger}$ was obtained using KS-DFT described in section S3. The equilibrium constant of the elementary reaction is given as

$$K_i(V) = \exp\left[-\frac{\Delta G_i(V)}{k_B T}\right] \tag{24}$$

where ΔG_i is the free energy change of the *i*th elementary reaction, whose value is also determined from the KS-DFT calculation described in section S3. Figure S1 shows the free energies of activations $\left(\Delta G_1^{\ddagger}, \Delta G_2^{\ddagger}\right)$ and reactions $\left(\Delta G_1, \Delta G_2\right)$ as a function of applied potential for Volmer and Heyrovsky steps.

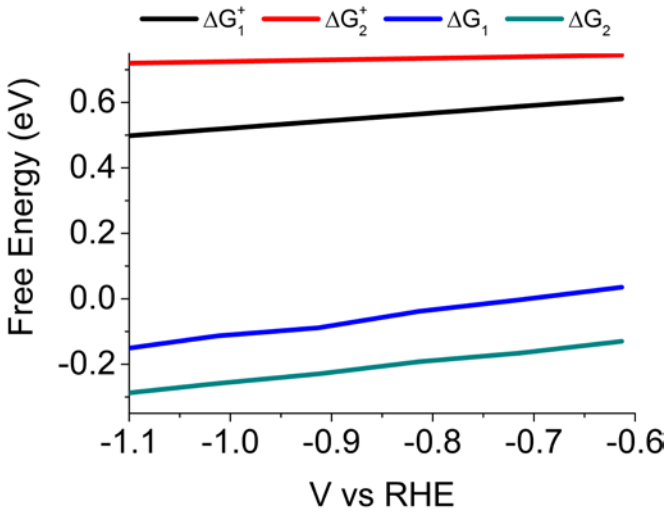

Figure S1: Dependence of free energies of activations $\left(\Delta G_1^{\ddagger}, \Delta G_2^{\ddagger}\right)$ and reactions $\left(\Delta G_1, \Delta G_2\right)$ on the applied potential for Volmer (subscript 1) and Heyrovsky (subscript 2) reactions

Figure 2 shows three different reaction mechanisms (RMs) for CO2RR over Ag(110), where RM-1, RM-2, and RM-3 involve $*H$, $**H_2O$, and free H_2O, respectively. The mathematical models for these three mechanisms are discussed in the subsequent sections.

S2.1 Reaction Mechanism-1

RM-1 involves a two-step mechanism for CO2RR over Ag(110),

$$*CO_2 + *H \underset{k_{-1}}{\overset{k_1}{\rightleftharpoons}} **COOH \tag{25}$$

$$**COOH + *H \underset{k_{-2}}{\overset{k_2}{\rightleftharpoons}} *CO + **H_2O \tag{26}$$

The rate expressions for these reactions are given as follows,

$$r_1 = k_1\left[\theta_{*CO_2}\theta_{*H} - \frac{1}{K_1}\theta_{**COOH}\right] \tag{27}$$

$$r_2 = k_2\left[\theta_{**\mathrm{COOH}}\theta_{*\mathrm{H}} - \frac{1}{K_2}\theta_{*\mathrm{CO}}\theta_{**\mathrm{H_2O}}\right] \tag{28}$$

The forward rate constants and the equilibrium constants were obtained from equations (23) and (24). Figure S2 shows the free energies of activations $\left(\Delta G_1^{\ddagger}, \Delta G_2^{\ddagger}\right)$ and reactions $\left(\Delta G_1, \Delta G_2\right)$ as a function of applied potential for reactions (25) and (26).

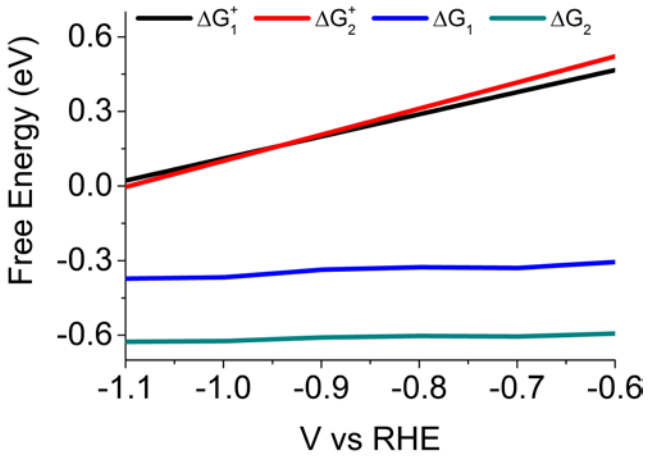

Figure S2: Dependence of free energies of activations $\left(\Delta G_1^{\ddagger}, \Delta G_2^{\ddagger}\right)$ and reactions $\left(\Delta G_1, \Delta G_2\right)$ on the applied potential for reduction of $*\mathrm{CO_2}$ (subscript 1) and $**\mathrm{COOH}$ (subscript 2) according to RM-1

Since the rates of adsorption and desorption are relatively faster than the rates of surface reactions, the adsorbed species such as $*\mathrm{CO_2}$, $*\mathrm{CO}$, $**\mathrm{H_2O}$, and $*\mathrm{H_2}$ were considered in quasi-equilibrium with their bulk concentrations, such that

$$\theta_{*\mathrm{CO_2}} = K_{*\mathrm{CO_2}}\, a_{\mathrm{CO_2}}\, \theta_* \tag{29}$$

$$\theta_{*\mathrm{CO}} = K_{*\mathrm{CO}}\, a_{\mathrm{CO}}\, \theta_* \tag{30}$$

$$\theta_{**\mathrm{H_2O}} = K_{**\mathrm{H_2O}}\, a_{\mathrm{H_2O}}\, \theta_*^2 \tag{31}$$

$$\theta_{*\mathrm{H_2}} = K_{*\mathrm{H_2}}\, a_{\mathrm{H_2}}\, \theta_* \tag{32}$$

where a_s is the activity of species *s* in the electrolyte at the cathode interface, and K_s is the equilibrium constant for adsorption/desorption of species *s* written as

$$K_s\left(V\right) = \exp\left[-\frac{\Delta G_s\left(V\right)}{k_B T}\right] \tag{33}$$

where ΔG_s is the free energy of adsorption of species *s* shown in Figure 3a.

The activity of H_2O in equation (31) is 1 because the electrolyte is dilute. The activity of CO_2 at the cathode was determined using the Continuum Transport model discussed in section S1. Since the gases are sparingly soluble in the water, their activities are equal to their mole fraction and they are assumed to be in equilibrium with the gases in the bubbles evolving at the cathode interface, such that

$$\begin{aligned} a_{\mathrm{CO_2}} &\approx x_{\mathrm{CO_2}} = K_{H,\mathrm{CO_2}}\, p_{\mathrm{CO_2}} \\ a_{\mathrm{CO}} &\approx x_{\mathrm{CO}} = K_{H,\mathrm{CO}}\, p_{\mathrm{CO}} \\ a_{\mathrm{H_2}} &\approx x_{\mathrm{H_2}} = K_{H,\mathrm{H_2}}\, p_{\mathrm{H_2}} \end{aligned} \tag{34}$$

where $K_{H,s}$ is Henry's constant for gaseous species dissolved in the electrolyte at 25 ^{o}C. Their values are $K_{H,\mathrm{CO_2}} = 33$ mM, $K_{H,\mathrm{CO}} = 0.93$ mM, and $K_{H,\mathrm{H_2}} = 0.78$ mM. The partial pressures of the product gases in equation (34) were determined from the flux balance at the cathode-electrolyte interface,

$$p_{\mathrm{CO}} = \frac{r_{\mathrm{CO}}}{r_{\mathrm{H_2}} + r_{\mathrm{CO}}}\, p_{\mathrm{T}} \tag{35}$$

$$p_{\mathrm{H_2}} = \frac{r_{\mathrm{H_2}}}{r_{\mathrm{H_2}} + r_{\mathrm{CO}}}\, p_{\mathrm{T}} \tag{36}$$

where r_{CO} is the rate of production of CO per unit area of the cathode, $r_{\mathrm{H_2}}$ is the rate of production of H_2 per unit area of the cathode, and p_T is the total pressure of the electrochemical cell. The value of p_T considered in all simulation was 1 atm.

The fractional coverage of $*\mathrm{H}$ was obtained by substituting equations (21), (22), (27), and (28) into the mass balance equation given as follows,

$$-r_1 - r_2 + r_3 - r_4 = 0 \tag{37}$$

Mass balance on species $**\mathrm{COOH}$ yields,

$$\theta_{**\mathrm{COOH}} = \frac{k_1 \theta_{*\mathrm{CO_2}} \theta_{*\mathrm{H}} + \dfrac{k_2}{K_2} \theta_{*\mathrm{CO}} \theta_{**\mathrm{H_2O}}}{\dfrac{k_1}{K_1} + k_2 \theta_{*\mathrm{H}}} \tag{38}$$

The fractional coverage of vacant sites $(*)$ was obtained from the site balance equation,

$$\theta_{*\mathrm{CO_2}} + \theta_{*\mathrm{CO}} + 2\theta_{**\mathrm{H_2O}} + \theta_{*\mathrm{H_2}} + 2\theta_{**\mathrm{COOH}} + \theta_{*\mathrm{H}} + \theta_{*} = 1 \tag{39}$$

The set of equations (29), (30), (31), (32), (37), (38), and (39) was solved simultaneously to determine fractional coverages θ_{*CO_2}, θ_{*CO}, θ_{**H_2O}, θ_{*H_2}, θ_{**COOH}, θ_{*H}, and θ_*. The calculated values of fractional coverages were substituted in the rates expression (26) to obtain rate of formation of CO,

$$r_{CO} = r_2 \tag{40}$$

and the partial current density of CO was calculated as follows,

$$i_{CO} = 2F\, r_{CO} \tag{41}$$

The rate of formation of H_2 was obtained by substituting the fractional coverages in reaction (20) ,

$$r_4 = r_{H_2} \tag{42}$$

and the partial current density of H_2 was calculated as follows,

$$i_{H_2} = 2F\, r_{H_2} \tag{43}$$

S2.2 Reaction Mechanism-2

RM-2 involves a two-step mechanism for CO2RR over Ag(110),

$$*CO_2 + **H_2O + e^- \underset{k_{-1}}{\overset{k_1}{\rightleftharpoons}} **COOH + * + OH^- \tag{44}$$

$$**COOH + **H_2O + e^- \underset{k_{-2}}{\overset{k_2}{\rightleftharpoons}} *CO + **H_2O + * + OH^- \tag{45}$$

The rate expressions for these reactions are given as follows,

$$r_1 = k_1\left[\theta_{*CO_2}\theta_{**H_2O} - \frac{1}{K_1}\theta_{**COOH}\,\theta_*\,x_{OH^-}\right] \tag{46}$$

$$r_2 = k_2\left[\theta_{**COOH}\theta_{**H_2O} - \frac{1}{K_2}\theta_{**H_2O}\theta_{*CO}\,\theta_*\,x_{OH^-}\right] \tag{47}$$

The forward rate constants and the equilibrium constants were obtained from equations (23) and (24). Figure S3 shows the free energies of activations $\left(\Delta G_1^{\ddagger}, \Delta G_2^{\ddagger}\right)$ and reactions $\left(\Delta G_1, \Delta G_2\right)$ as a function of applied potential for reactions (44) and (45).

The fractional coverages θ_{*CO_2}, θ_{*CO}, θ_{**H_2O}, and θ_{*H_2} are given by equations (29), (30), (31), and (32), respectively. The fractional coverage of $*H$ can was obtained by substituting equations (21), and (22) into the mass balance equation as follows,

$$r_3 - r_4 = 0 \tag{48}$$

which yields

$$\theta_{*\mathrm{H}} = \frac{k_3\,\theta_{**\mathrm{H_2O}} + \dfrac{k_4}{K_4}\theta_{*\mathrm{H_2}}\,x_{\mathrm{OH^-}}}{k_4 + \dfrac{k_3}{K_3}\theta_{*}\;x_{\mathrm{OH^-}}} \tag{49}$$

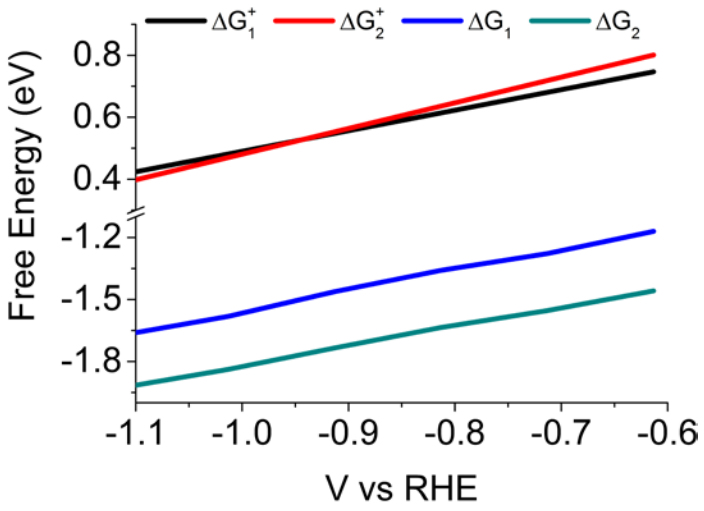

Figure S3: Dependence of free energies of activations $\left(\Delta G_1^{\ddagger}, \Delta G_2^{\ddagger}\right)$ and reactions $\left(\Delta G_1, \Delta G_2\right)$ on the applied potential for reduction of $*\mathrm{CO_2}$ (subscript 1) and $**\mathrm{COOH}$ (subscript 2) according to RM-2

Mass balance on species $**\mathrm{COOH}$ gives the fractional coverage,

$$\theta_{**\mathrm{COOH}} = \frac{k_1\theta_{*\mathrm{CO_2}}\theta_{**\mathrm{H_2O}} + \dfrac{k_2}{K_2}\theta_{**\mathrm{H_2O}}\theta_{*\mathrm{CO}}\,\theta_{*}\;x_{\mathrm{OH^-}}}{k_2 + \dfrac{k_1}{K_1}\theta_{**\mathrm{H_2O}}\theta_{*}\;x_{\mathrm{OH^-}}} \tag{50}$$

Fractional coverage of vacant sites was obtained from the site balance equation (39).

Equations (29), (30), (31), (32), (49), (50), and (39) was solved simultaneously to obtain fractional coverages $\theta_{*\mathrm{CO_2}}$, $\theta_{*\mathrm{CO}}$, $\theta_{**\mathrm{H_2O}}$, $\theta_{*\mathrm{H_2}}$, $\theta_{**\mathrm{COOH}}$, $\theta_{*\mathrm{H}}$, and θ_{*}.

The fractional coverages were substituted in the rates expression (47) to obtain rate of formation of CO,

$$r_{\mathrm{CO}} = r_2 \tag{51}$$

and the partial current density of CO was calculated using equation (41)

The rate of formation of H_2 was obtained by substituting fractional coverages into reaction (20)

$$r_4 = r_{H_2} \tag{52}$$

and the partial current density of H_2 was calculated using equation (43).

S2.3 Reaction Mechanism-3

RM-2 involves a three-step mechanism for CO2RR over Ag(110),

$$*CO_2 + \delta\ e^- \underset{k_{-0}}{\overset{k_0}{\rightleftharpoons}} *CO_2^{-\delta} \tag{53}$$

$$*CO_2^{-\delta} + * + H_2O + (1-\delta)\ e^- \underset{k_{-1}}{\overset{k_1}{\rightleftharpoons}} **COOH + OH^- \tag{54}$$

$$**COOH + H_2O + e^- \underset{k_{-2}}{\overset{k_2}{\rightleftharpoons}} *CO + H_2O + * + OH^- \tag{55}$$

The rate expressions for these reactions are given as follows,

$$r_0 = k_0\left[\theta_{*CO_2} - \frac{1}{K_0}\theta_{*CO_2^{-\delta}}\right] \tag{56}$$

$$r_1 = k_1\left[\theta_{*CO_2^{-\delta}}\theta_* - \frac{1}{K_1}\theta_{**COOH}\ x_{OH^-}\right] \tag{57}$$

$$r_2 = k_2\left[\theta_{**COOH} - \frac{1}{K_2}\theta_{*CO}\,\theta_*\ x_{OH^-}\right] \tag{58}$$

The forward rate constants and the equilibrium constants were calculated using equations (23) and (24). Figure S4 shows the free energies of activations $\left(\Delta G_0^{\ddagger}, \Delta G_1^{\ddagger}, \Delta G_2^{\ddagger}\right)$ and reactions $\left(\Delta G_0, \Delta G_1, \Delta G_2\right)$ as a function of applied potential for reactions (53), (54) and (55). The fractional coverages θ_{*CO_2}, θ_{*CO}, θ_{**H_2O}, θ_{*H_2}, and θ_{*H} are given by equations (29), (30), (31), (32), and (49) , respectively.

Mass balance on species $*CO_2^{-\delta}$ can give its fractional coverage as,

$$\theta_{*CO_2^{-\delta}} = \frac{k_0\theta_{*CO_2} + \frac{k_1}{K_1}\theta_{**COOH}\ x_{OH^-}}{\frac{k_0}{K_0} + k_1\theta_*} \tag{59}$$

Mass balance on species $**COOH$ yields,

$$\theta_{**COOH} = \frac{k_1 \theta_{*CO_2^{-\delta}} \theta_* + \frac{k_2}{K_2} \theta_{*CO} \theta_* \, x_{OH^-}}{k_2 + \frac{k_1}{K_1} x_{OH^-}} \tag{60}$$

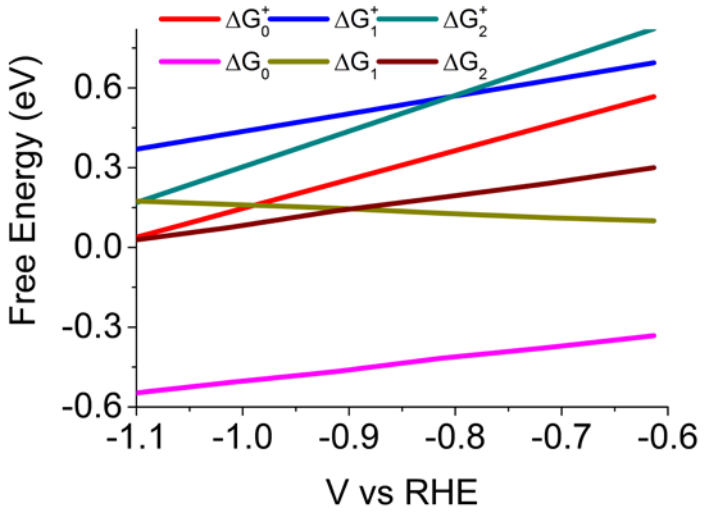

Figure S4: Dependence of free energies of activations $\left(\Delta G_0^{\ddagger}, \Delta G_1^{\ddagger}, \Delta G_2^{\ddagger}\right)$ and reactions $\left(\Delta G_0, \Delta G_1, \Delta G_2\right)$ on the applied potential for reduction of $*CO_2$ (subscript 0), $*CO_2^{-\delta}$ (subscript 1), and $**COOH$ (subscript 2) according to RM-3

The fractional coverage of vacant sites was obtained from the site balance,

$$\theta_{*CO_2^{-\delta}} + \theta_{*CO_2} + \theta_{*CO} + 2\theta_{**H_2O} + \theta_{*H_2} + 2\theta_{**COOH} + \theta_{*H} + \theta_* = 1 \tag{61}$$

The set of equations (29), (30), (31), (32), (49), (59), (60) and (61) was solved simultaneously to obtain fractional coverages $\theta_{*CO_2^{-\delta}}$, θ_{*CO_2}, θ_{*CO}, θ_{**H_2O}, θ_{*H_2}, θ_{**COOH}, θ_{*H}, and θ_*.

The fractional coverages were substituted in the rates expression (58) to obtain the rate of formation of CO,

$$r_{CO} = r_2 \tag{62}$$

and the partial current density of CO was calculated using equation (41)

The rate of formation of H_2 was obtained by substituting fractional coverages into reaction (20)

$$r_4 = r_{H_2} \tag{63}$$

and the partial current density of H_2 was calculated using equation (43).

S3. Kohn-Sham Density Functional Theory

All electronic structure calculations were performed using density functional theory (DFT) and were formed using a locally modified version of Vienna ab initio simulation program (VASP).(13-16) The Minnesota Local (M06-L) functional(17) and revised Perdew-Burke-Ernzerhof (RPBE) functional(18) were used in this study. The projector augmented-wave method(19, 20) were used in all DFT calculations. For RPBE calculations, the plane-wave cut-off was set to 300 eV and the and for M06-L calculations the plane-wave cut-off was set to 900 eV. Fermi-smearing width was set to 0.1 eV. A k-point sampling of (4,4,1) was used. The VASPsol program was used to describe the solvent with additional modifications to include electrolyte.(21-23) The dielectric constant of water was set to a relative permittivity of 78.4. The Debye length for the electrolyte was set to 3.0 Å, which corresponds to an electrolyte concentration of 1.0 M. Energy minimizations and transition state searches were stopped once the forces on each atom were less than 0.01 eV/Å. The transition state searches were performed using the Dimer method in the VTST package.(24) The convergence criterion for the electronic wavefunction was set to 10^{-6} eV.

Lattice constants of 4.08 Å were used for silver. The Ag(110) surface is represented by 3x4 atom configuration in the 110 surface configuration with 3 layers, for a total of 36 silver atoms. There are 21 Å of solvent/electrolyte between each surface plane.

The geometry was prepared in the following manner. Using the 3x4x3 silver atom model, the reactant (CO_2, $COOH_{ad}$, H_2O, and H_{ad}) was prepared with 48 water molecules. Figure S5 shows the geometry of adsorbed CO_2 ($*CO_2$) and adsorbed CO_2 anion $\left(*CO_2^{\delta-}\right)$. Using RPBE, 5ps of explicit water dynamics were performed. At the end of the molecular dynamics, geometry minimizations and transition state searches were performed using the M06-L functional.

Free energies of adsorbates were calculated by adding the zero-point energy (ZPE), entropies, and heat capacities to the electronic energy.(25) The frequencies were calculated by treating all of the degrees of freedom for the adsorbate as vibrational and that there were no significant changes in the vibrations of the Ag(110) surface. All vibrations were treated using the harmonic oscillator approximation. Several geometries had low-vibrational modes and these modes were reset to have a value of 50 cm^{-1}.

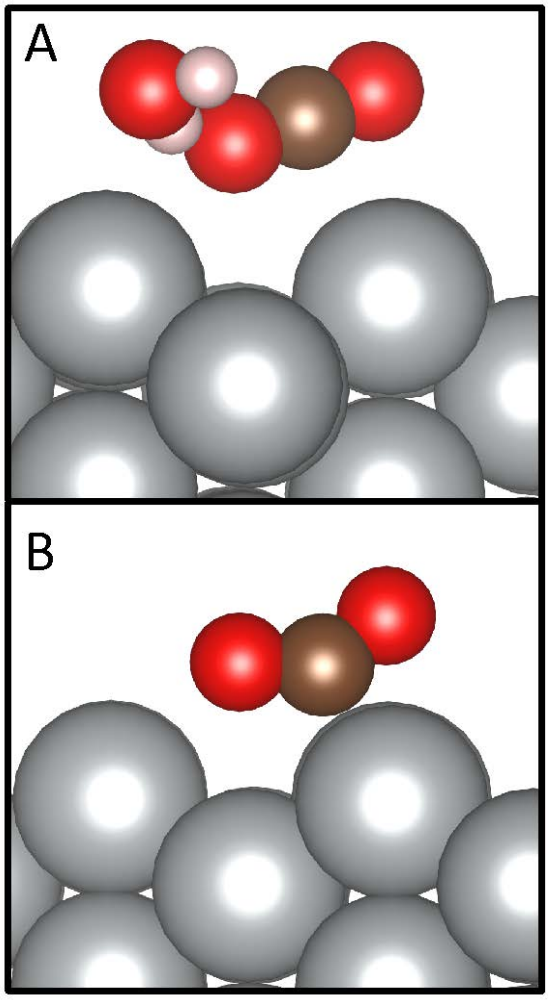

Figure S5: (A) The distorted adsorbed CO_2 ($*CO_2$) which has a bond angle of 178^o and bond lengths of 1.17 Å (hydrogen-bonded oxygen) and 1.16 Å. (B) The adsorbed CO_2 anion $\left(*CO_2^{\delta-}\right)$ species which has a bond angle of 140^o and bond lengths of 1.24 Å (left oxygen) and 1.22 Å (right oxygen).

S4. Multiscale Simulation

Figure S6 shows the algorithm for the multiscale simulation which couples continuum transport model, microkinetic model, and KS-DFT. The input for the simulation is the applied potential vs RHE to the cathode. The concentration of CO_2 $\left(c_{CO_2}\right)$ and pH are initialized using their respective bulk values. After initialization, the KS-DFT simulation was performed in VASP to obtain free energies of activation, reaction, and adsorption, which were used to calculate rate constants and equilibrium constants for each elementary reaction and adsorbates. The rate parameters were supplied to the microkinetic model to calculate partial current densities of products. The continuum model uses the partial current densities from the microkinetic model to

calculate the concentration of CO_2 and pH at the cathode-electrolyte interface. The simulation sequence was iterated until the convergence in the concentration of CO_2 and pH was achieved.

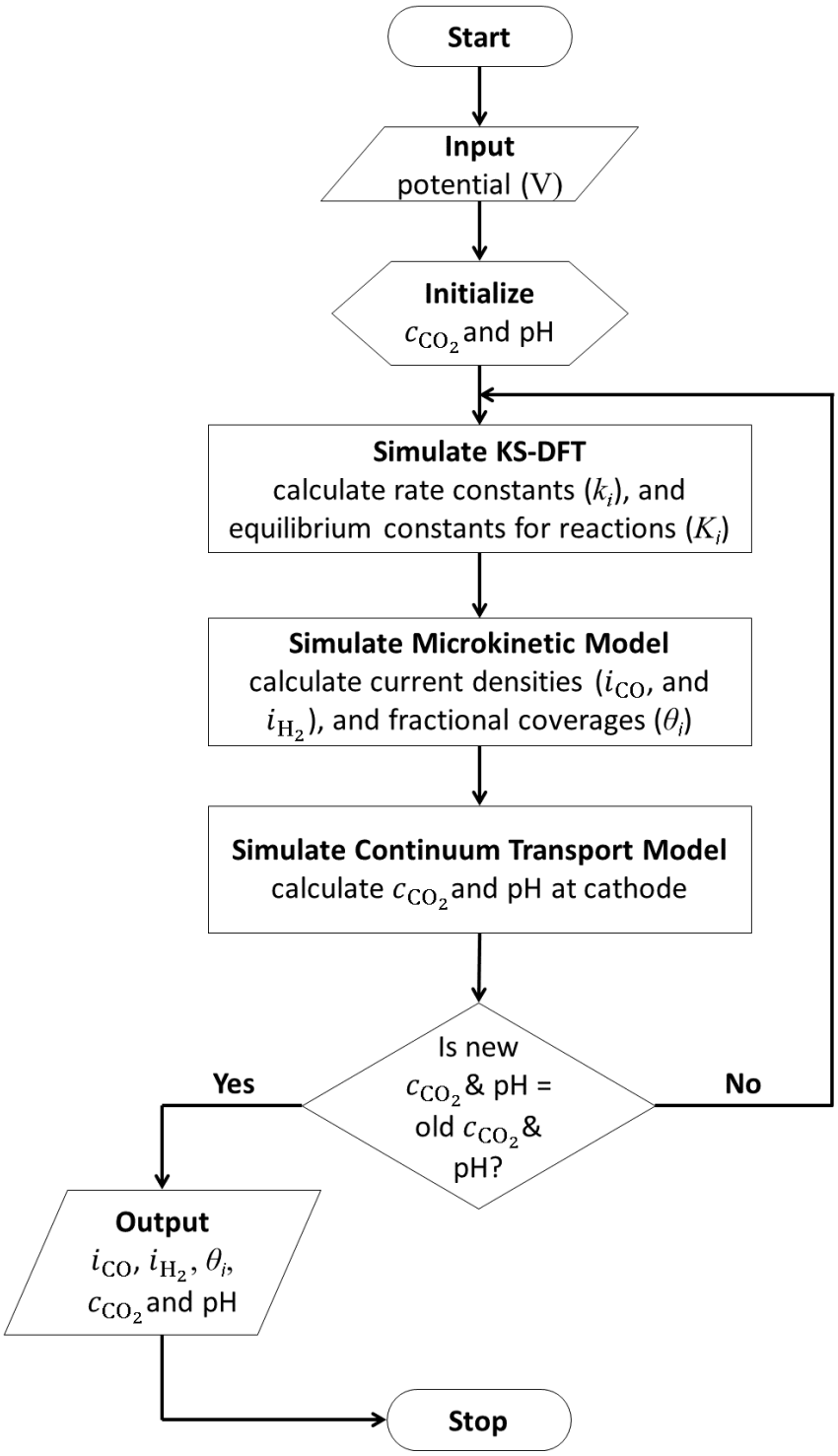

Figure S6: Multiscale simulation algorithm for simultaneous solution of KS-DFT, microkinetic model, and continuum transport model to predict partial current densities of CO2RR over Ag(110)

References

1. Riebesell U, Fabry VJ, Hansson L, & Gattuso J-P (2010) *Guide to best practices for ocean acidification research and data reporting* (Publications Office of the European Union Luxembourg).
2. Soli AL & Byrne RH (2002) CO_2 system hydration and dehydration kinetics and the equilibrium CO_2/H_2CO_3 ratio in aqueous NaCl solution. *Marine Chemistry* 78(2):65-73.
3. Schulz KG, Riebesell U, Rost B, Thoms S, & Zeebe R (2006) Determination of the rate constants for the carbon dioxide to bicarbonate inter-conversion in pH-buffered seawater systems. *Marine chemistry* 100(1):53-65.
4. Atkins P & De Paula J (2014) *Atkins' physical chemistry* (Oxford University Press).
5. Newman J & Thomas-Alyea KE (2012) *Electrochemical systems* (John Wiley & Sons).
6. Flury M & Gimmi TF (2002) Solute Diffusion. *Methods of Soil Analysis: Part 4 Physical Methods* (methodsofsoilan4):1323-1351.
7. Jähne B, Heinz G, & Dietrich W (1987) Measurement of the diffusion coefficients of sparingly soluble gases in water. *Journal of Geophysical Research: Oceans (1978–2012)* 92(C10):10767-10776.
8. Cents A, Brilman D, & Versteeg G (2005) CO_2 absorption in carbonate/bicarbonate solutions: The Danckwerts-criterion revisited. *Chemical Engineering Science* 60(21):5830-5835.
9. Hatsukade T, Kuhl KP, Cave ER, Abram DN, & Jaramillo TF (2014) Insights into the electrocatalytic reduction of CO_2 on metallic silver surfaces. *Physical Chemistry Chemical Physics* 16(27):13814-13819.
10. Le XT (2008) Permselectivity and microstructure of anion exchange membranes. *Journal of colloid and interface science* 325(1):215-222.
11. Kiss AM, *et al.* (2013) Carbonate and bicarbonate ion transport in alkaline anion exchange membranes. *Journal of The Electrochemical Society* 160(9):F994-F999.
12. Birss VI & Damjanovic A (1983) A study of the anomalous pH dependence of the oxygen evolution reaction at platinum electrodes in acid solutions. *Journal of The Electrochemical Society* 130(8):1694-1699.
13. Kresse G & Furthmüller J (1996) Efficient iterative schemes for *ab initio* total-energy calculations using a plane-wave basis set. *Physical Review B* 54(16):11169-11186.
14. Kresse G & Furthmüller J (1996) Efficiency of ab-initio total energy calculations for metals and semiconductors using a plane-wave basis set. *Computational Materials Science* 6(1):15-50.
15. Kresse G & Hafner J (1993) Ab initio molecular dynamics for liquid metals. *Physical Review B* 47(1):558-561.
16. Kresse G & Hafner J (1994) Ab initio molecular-dynamics simulation of the liquid-metal-amorphous-semiconductor transition in germanium. *Physical Review B* 49(20):14251-14269.
17. Zhao Y & Truhlar DG (2006) A new local density functional for main-group thermochemistry, transition metal bonding, thermochemical kinetics, and noncovalent interactions. *The Journal of Chemical Physics* 125(19):194101.
18. Hammer B, Hansen LB, & Nørskov JK (1999) Improved adsorption energetics within density-functional theory using revised Perdew-Burke-Ernzerhof functionals. *Physical Review B* 59(11):7413-7421.

19. Blöchl PE (1994) Projector augmented-wave method. *Physical Review B* 50(24):17953-17979.
20. Kresse G & Joubert D (1999) From ultrasoft pseudopotentials to the projector augmented-wave method. *Physical Review B* 59(3):1758-1775.
21. Letchworth-Weaver K & Arias TA (2012) Joint density functional theory of the electrode-electrolyte interface: Application to fixed electrode potentials, interfacial capacitances, and potentials of zero charge. *Physical Review B* 86(7).
22. Mathew K, Sundararaman R, Letchworth-Weaver K, Arias TA, & Hennig RG (2014) Implicit solvation model for density-functional study of nanocrystal surfaces and reaction pathways. *The Journal of chemical physics* 140(8):084106.
23. Fishman M, Zhuang HL, Mathew K, Dirschka W, & Hennig RG (2013) Accuracy of exchange-correlation functionals and effect of solvation on the surface energy of copper. *Physical Review B* 87(24):245402.
24. Henkelman G & Jónsson H (1999) A dimer method for finding saddle points on high dimensional potential surfaces using only first derivatives. *The Journal of chemical physics* 111(15):7010-7022.
25. Jinnouchi R & Anderson AB (2008) Electronic structure calculations of liquid-solid interfaces: Combination of density functional theory and modified Poisson-Boltzmann theory. *Physical Review B* 77(24).